



Enhanced the Catalytic activity of reduction of 4-nitrophenol on Ag/RGO nanocomposites

M. Khairy^{a,b,*}, Mohamed Mokhtar Mohamed^a, Ahmed Ibrahim^c

^aBenha University, Faculty of Science, Chemistry Department, Benha, Egypt

^bChemistry Department, College of Science, Al-Imam Mohammad Ibn Saud Islamic University, Riyadh, KSA

^cDuravit, Elmosheer Ahmed Ismail St., Sheraton Heliopolis, Piece No.9, Square 1160, Egypt

*Corresponding author: E-mail: mohkhairy@fsc.bu.edu.eg Tel: 0096652508917

Abstract

A simple deposition method was used to synthesize Ag@Ag₂O/RGO nanocomposites with different loads of Ag (0.4% and 4%) and at different annealing temperatures (250°C and 400°C). All samples were characterized with various techniques such as XRD, TEM-SAED, N₂ sorptiometry, Raman, FTIR, UV-Vis diffuse reflectance and photoluminescence spectroscopy. The catalytic performances of the samples towards reduction of 4-nitrophenol (4-NP) were tested under dark conditions. The XRD and TEM results revealed the well dispersion of Ag and Ag₂O moieties on RGO with crystallite size in the range of 17-34 nm. The nanocomposite Ag@Ag₂O/RGO annealed at 400°C exhibited the highest reduction rate constant for 4-NP reduction (0.01 s⁻¹), under the dark condition. The effect of presence of additives such as benzoquinone, triethanolamine, isopropyl alcohol and Na₂CO₃ on the reduction activity as well as its kinetics together with the reaction mechanism was well discussed.

Keywords: Ag₂O@Ag/RGO; Effect of Ag content; Catalytic activity; 4-Nitrophenol reduction.

Received; 19 Feb. 2018, Revised form; 8 Mar. 2018, Accepted; 8 Mar. 2018, Available online 1 Apr. 2018

1-Introduction

The reduction of 4-nitrophenol (4-NP) has received excess of attention due to the high toxicity and hazardous of P-nitrophenol to the health of human and the environment [1, 2]. Nitro-phenol and its derivatives result from the synthetic dyes production processes are sources of the aquatic pollution [3]. Various treatment methods such as adsorption, microbial degradation, Fenton method and photocatalytic degradation have been developed [4]. Recently, the reduction of P-NP via NaBH₄ in aqueous solution is important because it can be measured using UV-vis spectroscopy [5]. The reduction of 4-NP on metal nanoparticles such as Ag, Pd, Au, Pt-Ni, Pt, as well as their composites in aqueous solution under mild condition is particularly attractive [1].

Silver (Ag) nanoparticles are interesting due to their relatively low cost and superior properties such as high conductivity, antimicrobial and plasmon-resonant optical scattering properties [6, 7]. In particular, Ag nanoparticles have also been used in catalysis, and many excellent catalysts depend on Ag nanoparticles have been reported [8]. Ag nanoparticles can be immobilized on the surface of low cost and high surface area solid supports. Up to now, Ag nanoparticles have been immobilized onto various supports such as titania [9], activated carbon [10] and

carbon nanotube [11], etc. Recently, the appearance of graphene gives interesting technological applications [12]. Due to the unique two-dimensional structure of graphene and extraordinary physical properties such as huge surface area [13], superior electrical conductivity and high chemical stability [14], it is deemed as an ideal carbon support for evolving highly efficient catalysts [15]. It was reported that loading Ag nanoparticles onto graphene is not only prevent the restacking of graphene sheets and extend the application fields of graphene, but also enhance the catalytic activity of Ag nanoparticles due to the strong synergistic effect between the components of composites [16, 17]. Up to now, great attention has been paid on the synthesis of Ag/graphene oxide (GO) and Ag/reduced graphene oxide (RGO) hybrid materials.

In this work, the catalytic reduction of 4-nitrophenol on the Ag/RGO nanocomposites with different Ag contents at different annealing temperatures was studied. Accordingly, the nanocomposites were formed via reduction of silver ions by NaBH₄ in the presence of graphene oxide and a block copolymer as a stabilizer. The composites were thoroughly characterized using different tools such as XRD, FTIR, Raman TEM-SAED, UV-Vis diffuse reflectance and

N₂ sorption to illustrate the effect of temperature and silver content on enhancing the catalytic reduction activity

2. Experimental

2.1. Materials

All materials are analytical grade. Sodium nitrate (NaNO₃), potassium permanganate (KMnO₄), sulphuric acid (H₂SO₄) (98%), hydrogen peroxide (H₂O₂) 30%, de-ionized water, synperonic f108 (poly ethylene glycol-poly propylene glycol-block-poly ethylene glycol of an average M_n 2800), silver nitrate (AgNO₃) and sodium borohydride (NaBH₄) are obtained from Sigma Aldrich without further purification and Graphite (99%) was purchased from Fluka.

2.2. Preparation methods

2.2.1. Synthesis of graphene oxide and Ag/RGO nanocomposites.

Graphene oxide (GO) was prepared from natural graphite according to a modification of the Hummers–Offeman method [18]. The detailed procedure for synthesizing the Ag/RGO nanocomposites via a simple deposition method was as follow: 2 g of GO is suspended in 10 ml of deionized water. 5×10^{-3} M of silver nitrate solution was prepared by dissolving 0.0085 g in 10 ml and added to the GO suspension dispersed in 10 ml of the block copolymer (10 g/ml) solution that left under stirring for 30 min followed by sonication for 1/2 h. 100 ml of 0.1M NaBH₄ solution was added dropwise to the previous prepared mixture under heating at 80 °C for 1h. The mixture color was changed to a deep yellow color. The obtained precipitate was filtered and washed several times with distilled water. The precipitate was dried in an oven at 100°C for 5 h. The obtained powder was heated finally at 400°C to obtain 0.4 wt% Ag/RGO₄₀₀ that denoted as 0.4Ag/RGO₄₀₀. The other composites with Ag content of 4 wt% were prepared with the same procedure with different amount of AgNO₃ and the obtained powder was heated at 250 and 400°C to obtain Ag(4%)/Go₂₅₀ and Ag(4%)/Go₄₀₀, samples those respectively denoted as 4Ag/RGO₂₅₀ and 4Ag/RGO₄₀₀.

2.3. Characterization tools

The X-ray diffraction was measured at room temperature via a Philips diffractometer of Model PW-3710. The diffraction patterns were carried out with Ni-filtered Cu K α radiation ($\lambda=1.541$ Å) at 36 kV. The Fourier transform infrared (FT-IR) spectra were monitored via a double beam Perkin Elmer Spectrometer. Raman spectra were measured with a U-1000 laser Raman spectrometer using the 514.5 nm line of an ArC laser as the excitation beam. The surface texturing properties and the pore size distribution were determined from N₂ adsorption isotherms taken at 77 K using a conventional volumetric apparatus and from the desorption branch of isotherm using BJH analysis, respectively. UV–Vis JASCO spectrophotometer, V-570 was used to determine the diffuse reflectance ultraviolet–visible spectroscopy (UV–vis DRS) of the samples. TEM and selected area electron diffraction (SAED) were measured using a JEM-2100 model at an accelerating voltage of 120 kV. Thermo scientific fluorescence

spectrophotometer model Lumina was used to measure the photoluminescence (PL) spectra. The measurements were carried out using a He/Cd laser (310 nm) as an excitation source at room temperature.

2.4. Catalytic activity measurements

The catalytic activity of synthesized nanocomposites was tested via catalytic reduction; 12.5 ml of 0.5 M of NaBH₄ was added to 100 ml of 0.1mmol aqueous solution of the 4-nitrophenols under constant stirring. The yellow colour of the solution was darkened with the addition of NaBH₄, due to the formation of phenolate ions. Then 0.025 mg catalysts were added under stirring to the previous solution. The reduction of nitrophenol was observed via disappearing the dark yellow colour of the solution. The reaction progress was tested at different time intervals. The formation of aminophenol from the reduction of nitrophenol was checked by measuring the absorption maxima corresponding to nitrophenol as well as the product aminophenol via UV-Visible spectroscopy (a Perkin Elmer Lambda-900). After the completion of the reaction, the catalyst was separated by filtration.

3. Results and discussion

3.1. XRD

XRD patterns of Ag/RGO nanocomposites at different Ag contents and different annealing temperatures namely 0.4Ag/RGO₄₀₀, 4Ag/RGO₂₅₀, and 4Ag/RGO₄₀₀ nanocomposites are given in Fig.1. Fig. 1 shows the XRD patterns of graphene oxide. Graphene oxide XRD pattern reveals the main diffraction peaks at 11.1° and 43.8° related to (002) and (100) reflections planes. It was observed for all Ag/RGO nanocomposites that the diffraction peak of graphene oxide at 12.5° was vanished and the peaks at 24.5° and 43.8° due to (002) and (100) reflections of reduced graphene [19, 20] were appeared pointing to the graphene oxide reduction during the addition of sodium borohydride and thermal treatment processes. The XRD pattern of 0.4Ag/RGO₄₀₀ nanocomposite reveals peaks at 25.6° and 20.2° indicating the presence of RG [19] as well as appearance of peaks at 38.1°, 44.64° and 64.8° indexed to the (111), (200) and (220) crystallographic planes of the face centered cubic (FCC) of Ag nanoparticles, respectively (JCPDS card no. 89-3722 and 65-2871). Additionally, peaks at $2\theta = 30.4^\circ$ and 38.1° are assigned to (120) and (200) planes of well-crystallized cubic Ag₂O, respectively (JCPDS No, 41-1104 and 76-1393). The presence of the graphene peak in the nanocomposites patterns also indicates that Ag/Ag₂O nanoparticles are successfully loaded onto the graphene surface. The reduction of Ag⁺ to Ag is facilitated by the presence of various functional groups on GO surface [21, 22]. This groups on GO can act as nucleation sites i.e. excess of small aromatic conjugated groups on GO can act as an electron-donating source to reduce Ag ions into Ag NPs [23]. In addition, the GO-Ag⁺ complex was formed when GO was suspended in aqueous solution containing Ag⁺ ions, via electrostatic interaction between the Ag⁺ cation and the negatively charged GO leading to strong adsorption of Ag⁺ with surface of GO.

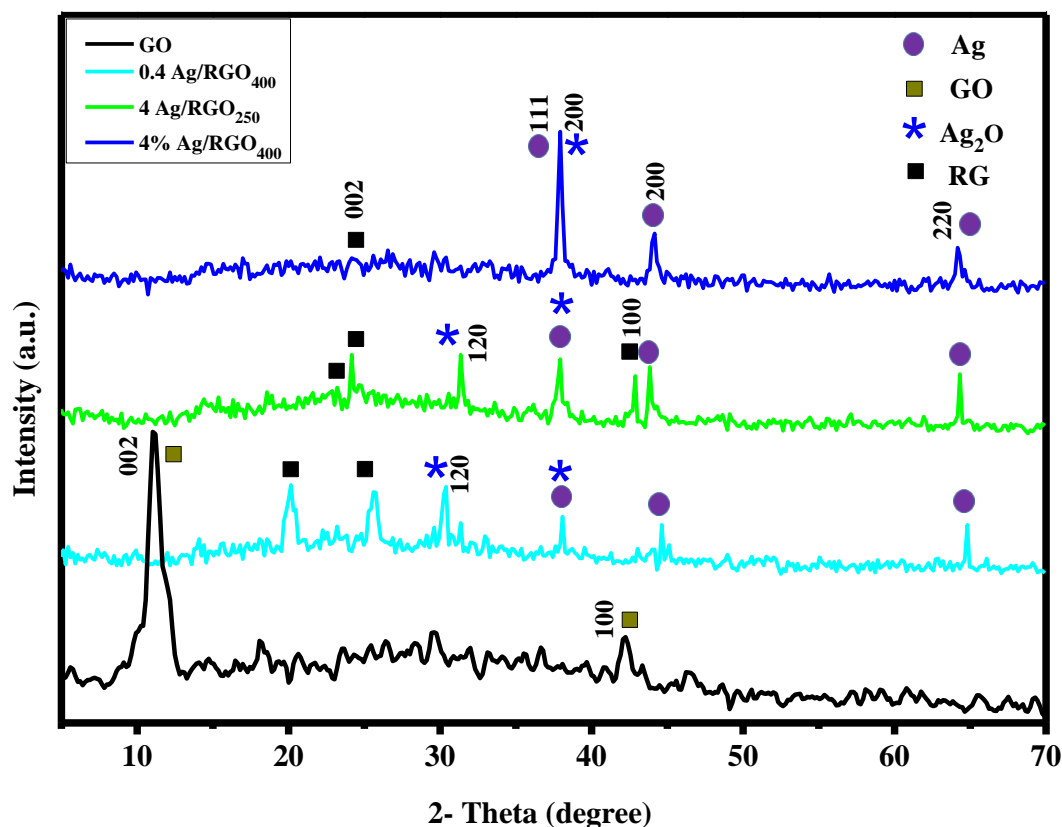


Fig (1): XRD patterns of GO, 0.4%Ag/RGO₄₀₀, 4% Ag/RGO₂₅₀ and 4%Ag/RGO₄₀₀ catalysts.

Subsequently, when NaBH₄ (reducing agent) was added to the previous solution, Ag⁺ ions were in-situ gradually reduced to Ag NPs beside GO reduction to reduced graphene. The presence of Ag₂O phase may be due to relative oxidation of Ag NPs by reaction with O₂ from the air at the liquid-air interface, and form Ag₂O [24]. This also indicates that the silver particles itself are relatively oxidized while GO is relatively reduced.

On increasing the Ag content from 0.4% to 4% in the Ag/RGO nanocomposite annealed at 400°C, the intensity of the peaks is increases; as precisely observed for the (111) facet. Besides, vanishing the peak at 30.4° illustrates a decrease of the Ag₂O species, suggesting its partial reduction. The 4Ag/RGO₄₀₀ sample also shows a decrease in the graphene peak intensity suggesting slight distortion of graphene layers probably due to the high dispersion of Ag nanoparticles and high annealing temperature (400°C). The crystallites size of 0.4Ag/ RGO₄₀₀, 4Ag/ RGO₂₅₀ and 4Ag/ RGO₄₀₀ were respectively 37, 25 and 39 as calculated using the Debye-Scherrer equation [25].

3.2. Surface textural

HR-TEM and SAED analyses were used for examining the surface morphology and the distribution of 0.4Ag/RGO₄₀₀, 4Ag/RGO₂₅₀, and 4Ag/RGO₄₀₀ nanocomposites (Fig. 2). The TEM image of 0.4Ag

/RGO₄₀₀ (Fig. 2a) shows a randomly paper-like sheet structure related to RGO with spherical dark spots of Ag and light spots of Ag₂O nanoparticles, those are well homogeneously dispersed on the RGO nanosheets surface without significant aggregation. It was found that, the average particle size of Ag@Ag₂O nanoparticles is approximately 19 nm. In addition, a typical selected area electron diffraction (SAED) pattern exhibits many-crystal diffraction features of the 0.4Ag/GO₄₀₀ composite (Fig. 2a). The SAED pattern shows three visible diffraction rings; the first diffraction ring with a lattice spacing of 0.145 nm is correspond to the (220) plane of the face centered cubic Ag [26]. The second ring at 0.237 nm is likely attributed to the (200) reflection of the cubic Ag₂O moieties. Another diffraction ring is also observed and indexed to the (002) facet of reduced graphene, giving an indication about the good contact between Ag@Ag₂O NPs with the graphene nanosheets. This was in conformity with the results obtained from XRD. The TEM image of 4Ag/RGO₂₅₀ (Fig. 2b) reveals well dispersion of spherical silver nanoparticles with some aggregation of Ag and Ag₂O on graphene nanosheets. The Ag and Ag₂O nanoparticles with size 34 nm were well distributed on the graphene nanosheet surface. The increase in particle size may be due to high concentration of Ag.

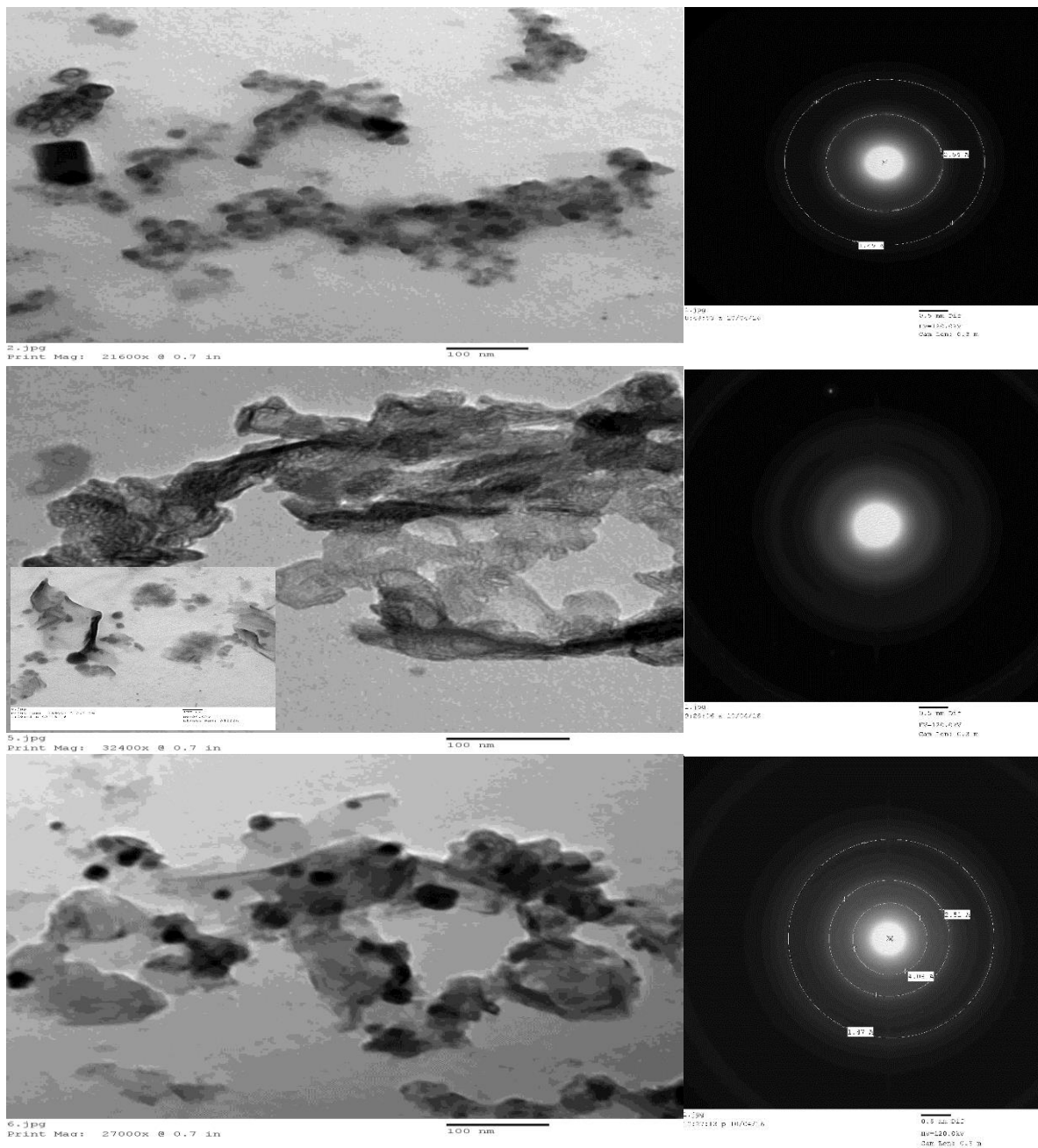


Fig (2): TEM and SAED images of a) 0.4%Ag/RGO₄₀₀ b) 4%Ag/RGO₂₅₀ and c) 4% Ag/RGO₄₀₀

The SAED pattern shows rings that related to lattice fringes (002), (200) and (220) from interior to exterior and indexed respectively to graphene, Ag₂O and Ag particles. This suggests the well dispersion of Ag nanospheres and Ag₂O on graphene and emphasizes the strong interaction between them. On the other hand, on increasing the annealing temperature of the sample 4% Ag to 400°C (4Ag/RGO₄₀₀) (Fig. 2c), the graphene sheet structure was almost disintegrated and distorted as confirmed from XRD results, with well distribution of the silver nanospheres on its surface with some nanoparticles aggregation. The particle size of the Ag nanoparticles was 17 nm almost half of that annealed at 250°C. The SAED pattern indicates rings

that offers lattice fringes (002), (200) and (200) indexed respectively, to RGO, Ag₂O and Ag.

3.3. FTIR and Raman spectroscopy

FTIR spectra of GO and 0.4Ag/RGO₄₀₀, 4Ag/RGO₂₅₀ and 4Ag/RGO₄₀₀ nanocomposites are shown in Fig. 3. For GO, the wide peak centered at 3421 cm⁻¹ is assigned to the O-H stretching vibrations while the peaks at 1718, 1620, 1382, and 1225, 1161 and 1049 cm⁻¹ are attributed to C=O stretching, C=C sp²-hybridized group and bending O-H, stretching C-OH and stretching C-O-C, respectively [27]. In addition, the peaks at 1049 and 1161cm⁻¹ can be related to C-O vibration of alkoxy or epoxy groups [28]. The peaks at 2853 and 2923 cm⁻¹ are related to symmetric and asymmetric stretching vibration of CH₂ groups,

respectively [27]. A peak at 500 cm^{-1} due to the O-H bending vibration is also observed. The IR spectrum of the $0.4\text{Ag}/\text{RGO}_{400}$ composite shows a band at 1586 cm^{-1} assigned to the aromatic C=C vibrations of unoxidized graphitic carbon, to suggest the reduction of GO [28, 29] in addition to the peak at 1436 cm^{-1} which is indexed to O-H bending [27]. The peaks at 1344 , 1278 , 1131 and 1001 cm^{-1} are red shifted when compared to those appeared in GO at 1382 , and 1225 , 1161 and 1049 cm^{-1} with noticeable decrease in the intensity of all peaks. It was observed that the peaks at 1718 and 1620 cm^{-1} were disappeared which indicates that the carbonyl group and O-H groups were

removed due to the reduction process [30]. The peak at 3382 cm^{-1} attributed to the stretching vibration of O-H bonds of absorbed water molecules is red shifted for the Ag/RGO composite. In addition, appearing of new peaks at 945 , 879 and 826 cm^{-1} arise from multi-phonon processes in Ag_2O are depicted [31]. Also, the peaks at 709 , 626 and 464 cm^{-1} are respectively attributed to the CH_2 rocking modes of the surfactant pluronic [32], metallic Ag and $\nu_{\text{as}}(\text{Ag-O})$ stretching mode incorporated within the RGO structure [33, 34]. The observed vibrational bands at low frequency region $945\text{-}464\text{ cm}^{-1}$ suggested the formation of Ag_2O NPs [35].

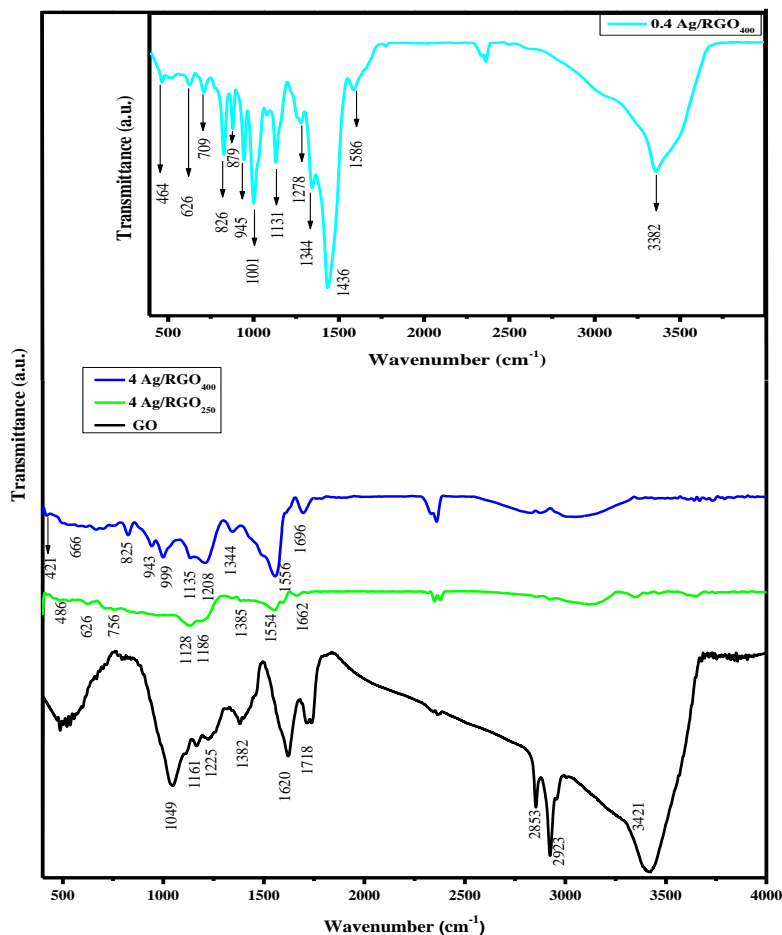


Fig (3): FTIR spectra of GO, 0.4% Ag/RGO₄₀₀, 4% Ag/RGO₂₅₀, 4% Ag/RGO₄₀₀ and in the $400\text{-}4000\text{ cm}^{-1}$ range

The intensity loss of the peak at around 3400 cm^{-1} confirms the participation and decreasing of function groups containing oxygen in the Ag nanoparticles formation. In addition, it also confirms that strong interactions may occur between Ag and Ag_2O nanoparticles and the remaining surface O atoms of hydroxyl group [36].

The FTIR spectra of $4\text{Ag}/\text{RGO}_{400}$ composite, shows peaks at 1696 , 1556 , 1344 , 1208 , 1135 and 999 cm^{-1} which red shifted and decreased in their intensity from that appeared in GO at 1718 , 1382 , 1225 , 1161 and 1049 cm^{-1} beside the approximate disappearing of the peak at 1718 cm^{-1} , suggesting reduction of GO. Besides, the appearance of peaks similar to those appeared in $0.4\text{Ag}/\text{RGO}_{400}$ at 943 , 825 , 666 and 421 cm^{-1} related to multi-phonon processes in

Ag_2O , metallic Ag and $\nu_{\text{as}}(\text{Ag-O})$ stretching mode incorporated within the RGO structure, respectively. It was found that on increasing the silver content to 4%, the peaks intensities are almost decreased and red shifted which indicate the well interaction of Ag and Ag_2O with graphene. The FTIR spectrum of $4\text{Ag}/\text{RGO}_{250}$ composite shows decrease in the intensities of all peaks that appeared at 1662 , 1554 , 1385 , 1186 and 1128 cm^{-1} in addition to very small peaks at 756 , 626 and 486 cm^{-1} . These results indicate the effective reduction of GO and well interaction between Ag and graphene structure.

Raman is a very useful tool for having information on the graphitic materials, their level of graphitization, defect amounts and the identification of layer structure [37, 38].

The 2D peak at about 2700 cm^{-1} as well as the intensity ratio of G (at 1600 cm^{-1}) to 2D peak can be used to evaluate the layer structure of graphene. The structure of graphene sheet and its interaction with Ag can be proven by measuring the Raman spectra of GO as well as those of $0.4\text{Ag}/\text{RGO}_{400}$, $4\text{Ag}/\text{RGO}_{250}$, and $4\text{Ag}/\text{RGO}_{400}$ nanocomposites, (Fig. 4). The Raman spectra related to GO show peaks at 1349 , 1600 and 2800 cm^{-1} , which assigned to the breathing mode of A_{1g} symmetry involving phonons near the K zone boundary (D band), the E_{2g} mode of sp^2 -bonded carbon atoms (G band) and the second order of the D band (2D) of graphene characteristics of two-phonon lattice vibration process, respectively [39].

On the other hand, the Raman spectra of all Ag/RGO nanocomposites show bands in range of 1352 - 1357 cm^{-1} (due to D bands vibration) signifying disordered graphite planes and defects [40], and bands in the range of 1589 - 1596 cm^{-1} (G band), in addition to the 2D band extending from 2643 to 2956 cm^{-1} with the similar shape and position. The Raman spectra of all Ag/RGO composites shows that the D bands are shifted to higher wavenumbers (1352 - 1357 cm^{-1}) where the G band is shifted to lower wavenumbers (1589 - 1596 cm^{-1}) compared to GO 1349 and 1600 cm^{-1} ,

respectively. This is indication to the reduction of GO and well interaction between Ag and Ag_2O with graphene [41, 42].

The disorder and the defects in the graphitic layers are measured from the intensity ratio of D and G peaks (I_D/I_G). It was found that the intensity ratios ($I(D)/I(G)$) of $0.4\text{Ag}/\text{RGO}_{400}$, $4\text{Ag}/\text{RGO}_{250}$ and $4\text{Ag}/\text{RGO}_{400}$ nanocomposites are 1.15 , 1.04 and 1.03 respectively, which are greater than that of GO (0.93), confirming a relative high imperfection level in the RG due to Ag incorporation. It is clear that $4\text{Ag}/\text{RGO}_{250}$ and $4\text{Ag}/\text{RGO}_{400}$ nanocomposites show the lowest intensity ratio compared to other composites indicating the lowest degree of imperfections in these samples. The presence of 2D band in all the synthesized nanocomposites indicates the multi-layered structure of the synthesized graphene. From the intensity ratio of 2D and G peaks (I_{2D}/I_G), it can precise measure the graphitic layers. It was found that, the I_{2D}/I_G intensity ratio of GO (0.22) decreased than those of $4\text{Ag}/\text{RGO}_{250}$ (0.63) and $4\text{Ag}/\text{RGO}_{400}$ (0.75) but was higher than that of $0.4\text{Ag}/\text{RGO}_{400}$ (0.19). This indicates that incorporation of Ag increases the number of layers of graphene in the nanocomposites.

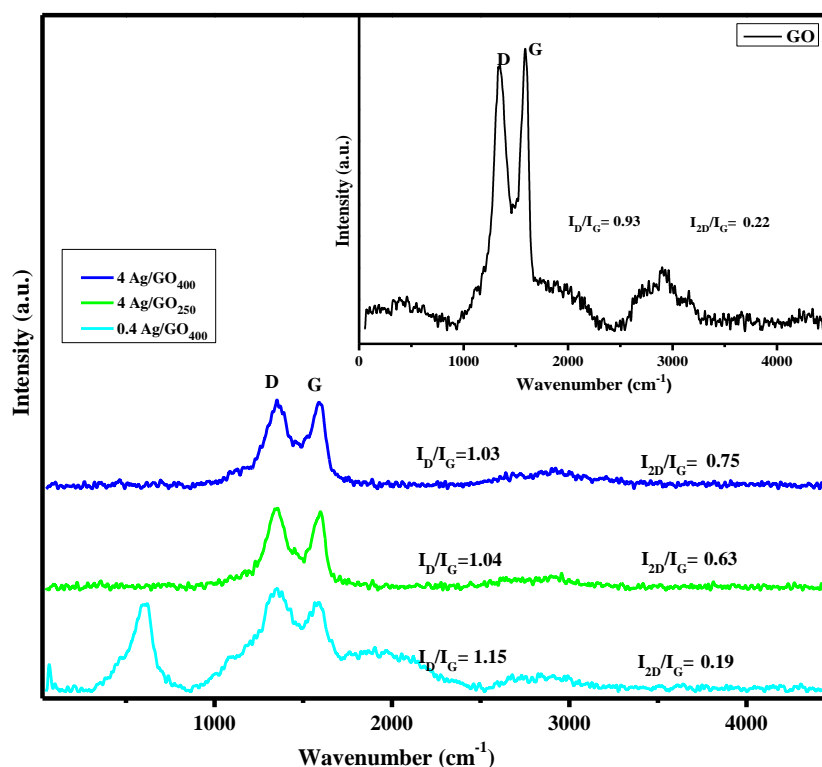


Fig (4): Raman spectra of GO, $0.4\text{Ag}/\text{RGO}_{400}$, $4\text{Ag}/\text{RGO}_{250}$ and $4\text{Ag}/\text{RGO}_{400}$ catalysts.

3.4. Texturing properties

The surface texturing of the prepared Ag/RGO nanocomposites is studied by the N_2 adsorption/desorption isotherm, as given in Fig. 5, where the inset is the pore size distribution plots determined according to the Barrett-Joyner-Halenda (BJH) analysis. The isotherms show typical type IV with H_3 type hysteresis loop, according to IUPAC classification [43]. These isotherms suggest the

mesoporous structure of all samples and characterizing aggregates of plate-like or slit-shaped pores [43]. The hysteresis loops of the samples close at P/P_0 values of 0.45 , 0.42 , 0.45 , and 0.45 for GO, $0.4\text{Ag}/\text{RGO}_{400}$, $4\text{Ag}/\text{RGO}_{250}$ and $4\text{Ag}/\text{RGO}_{400}$ nanocomposites, respectively. These suggest the presence of similar large pores in all the samples. It was found that the surface area of GO (176.1

m²/g) was greater than all nanocomposites (0.4Ag/RGO₄₀₀: 78.6 m²/g, 4Ag/RGO₂₅₀: 43.6 m²/g and 4Ag/RGO₄₀₀: 71.4 m²/g). It was observed that surface area increases with increasing both of Ag content and annealing temperature

suggesting their great effects. On the other hand, the pore radius for the composites annealed at 400°C were lower than that annealed at 250°C (0.4Ag/RGO₄₀₀: 12.3 Å, 4Ag/RGO₄₀₀: 18.75 Å) and (4Ag/RGO₂₅₀: 19.24 Å).

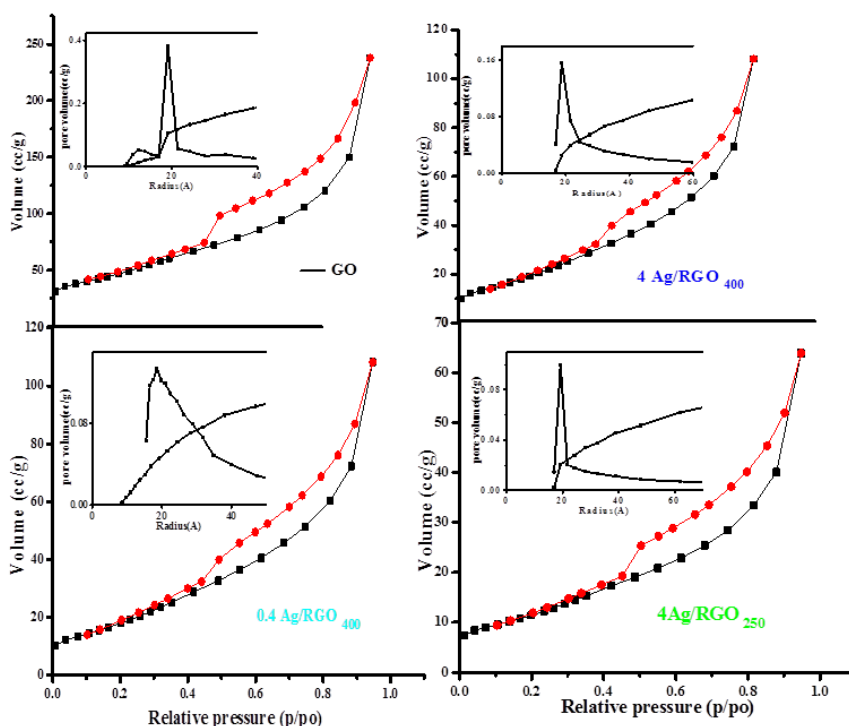


Fig (5): Adsorption-desorption isotherms and pore size distribution curves (in-set) of GO, 0.4% Ag/RGO₄₀₀, 4% Ag/RGO₂₅₀ and 4% Ag/RGO₄₀₀.

The pore size distribution curves have shown that the Ag incorporation shows only a one modal type of pore localized mostly at 20 Å. On the same time, these samples have extended their mesoporous size to be at 143 Å for 0.4% Ag/RGO₄₀₀, 150 Å for 4% Ag/RGO₂₅₀ and 145 Å for 4% Ag/RGO₄₀₀, respectively. In contrast, the pore volume for the composites annealed at 400°C were higher than those annealed at 250 °C (0.4Ag/RGO₄₀₀: 0.111 cm³/g, 4Ag/RGO₄₀₀: 0.167 cm³/g) and (4Ag/RGO₂₅₀: 0.098 cm³/g). This may be due to the particles size of Ag and Ag₂O in the composites annealed at 400°C were lower than those in the composites annealed at 250°C and this indicates the well dispersion of Ag nanoparticles in the graphene structure.

3.5. UV-Vis diffuse reflectance

Fig. 6 shows the UV-visible absorption spectra measured for GO, 0.4Ag/RGO₄₀₀, 4Ag/RGO₂₅₀ and 4Ag/RGO₄₀₀ nanocomposites. It was observed that the absorption spectra of 4Ag/RGO nanocomposite annealed at 250°C showed characteristic surface plasmon resonance (SPR) broad band at wavelengths 400 nm, respectively, indicating the presence of Ag nanoparticles on RGO surface [44]. This broad SPR band for the Ag NPs verified the formation of large spherical Ag NPs, as matched with the TEM results.

On the other hand, the absorption spectra of 0.4Ag/RGO₄₀₀ and 4Ag/RGO₄₀₀ show absorption peaks at 365 nm and 375 nm characterizing the surface plasmon resonance (SPR) band of Ag NPs [44]. The spectra show also sharp peak at 340 nm which may be related to the n-π* transition of the C=C bonds in RGO. The SPR band is shifted to lower wavelength compared to the previous samples which may be due to lower particle size of Ag nanoparticles of these samples compared to others, as confirmed from TEM [45]. It was observed that at the range of wavelength from 495 to 900 nm, both 4Ag/RGO₂₅₀ and 4Ag/RGO₄₀₀ nanocomposites show high absorption of visible light, suggesting that these two composites may give higher catalytic or photocatalytic activity under the same light irradiation.

The optical band gap is determined using the following relationship [46]

$$(\alpha h\nu)^{1/n} = B (h\nu - E_g) \quad (1)$$

The E_g-value is calculated using the least square fitting of Eq. (1) and in the inset in Fig. 6. The energy gap values of the 0.4Ag/RGO₄₀₀, 4Ag/RGO₂₅₀ and 4Ag/RGO₄₀₀ nanocomposites are 1.5, 1.6, 1.55, 1.62 eV, respectively. This small energy gap values indicate the well interaction between Ag and Ag₂O exhibiting continuous strong absorption of visible light with graphene.

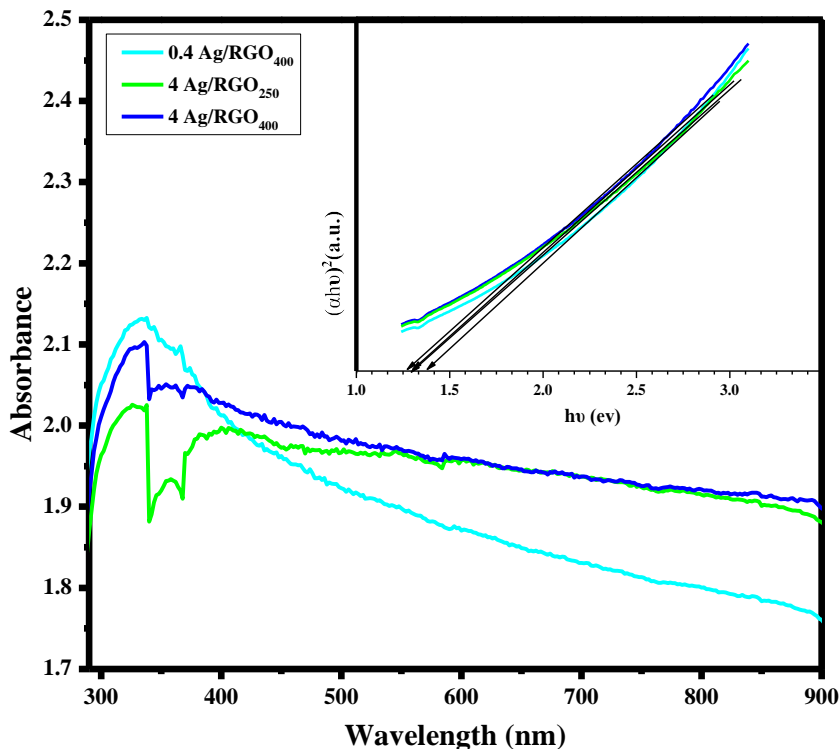


Fig (6): UV-visible spectra of 0.4%Ag/RGO₄₀₀, 4%Ag/RGO₂₅₀ and 4%Ag/RGO₄₀₀ catalysts. besides Band gap energy as in-set.

3.6. Photoluminescence emission (PL)

The lifetime of electron-hole pair has a paramount effect on the photocatalytic process. The photoluminescence (PL) of 0.4Ag/RGO₄₀₀, 4Ag/RGO₂₅₀ and 4Ag/RGO₄₀₀ nanocomposites is carried out at room temperature using the 225 nm excitation (Fig. 7).

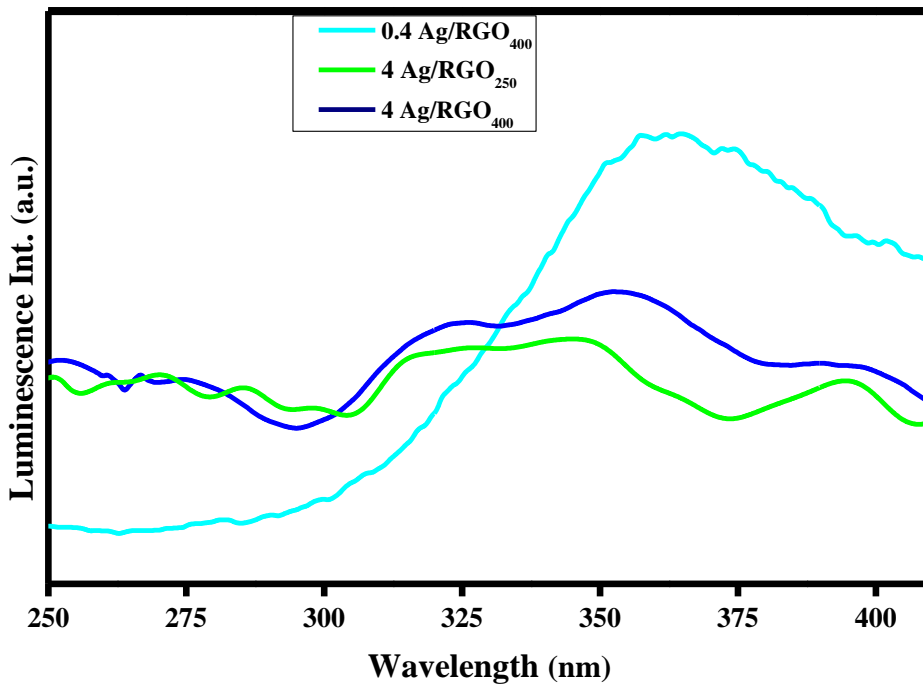


Fig (7): Photoluminescence emission spectra of 0.4%Ag/RGO₄₀₀, 4%Ag/RGO₂₅₀ and 4%Ag/RGO₄₀₀ catalysts excited at 310 nm.

The 0.4Ag/RGO₄₀₀, 4Ag/RGO₂₅₀ and 4Ag/RGO₄₀₀ nanocomposites displayed strong and broad emission peaks around 350-365 nm which may be due to surface defects in the functional groups of the RGO and edge structure [47]. The peak is shifted from 365 cm⁻¹ in 0.4Ag/RGO₄₀₀ to 355 cm⁻¹ in 4Ag/RGO₄₀₀, to 348 cm⁻¹ in 4Ag/RGO₂₅₀ sample. The emission intensity is significantly decreased over all the range in the order 4Ag/RGO₄₀₀ > 4Ag/RGO₂₅₀. This possibly indicates that 4Ag/RGO₄₀₀ and 4Ag/RGO₂₅₀ samples acted as photo-induced charge carrier's traps suggesting a high expected photocatalytic activity.

3.7. P-Nitrophenol catalytic reduction

The catalytic activity of the synthesized nanocomposites was evaluated by measuring the catalytic reduction of p-nitrophenol by NaBH₄. A typical plot of nitrophenol absorbance as a function of wavelength on the 4Ag/RGO₄₀₀ nanocomposite was represented in Fig. 8. The Figure shows the absorption band related to p-nitrophenolate ion at 400 nm in presence of NaBH₄ [48], which decreases rapidly with the time progress with appearance and increase of a new peak at 300 nm due to the 4-AP formation [49].

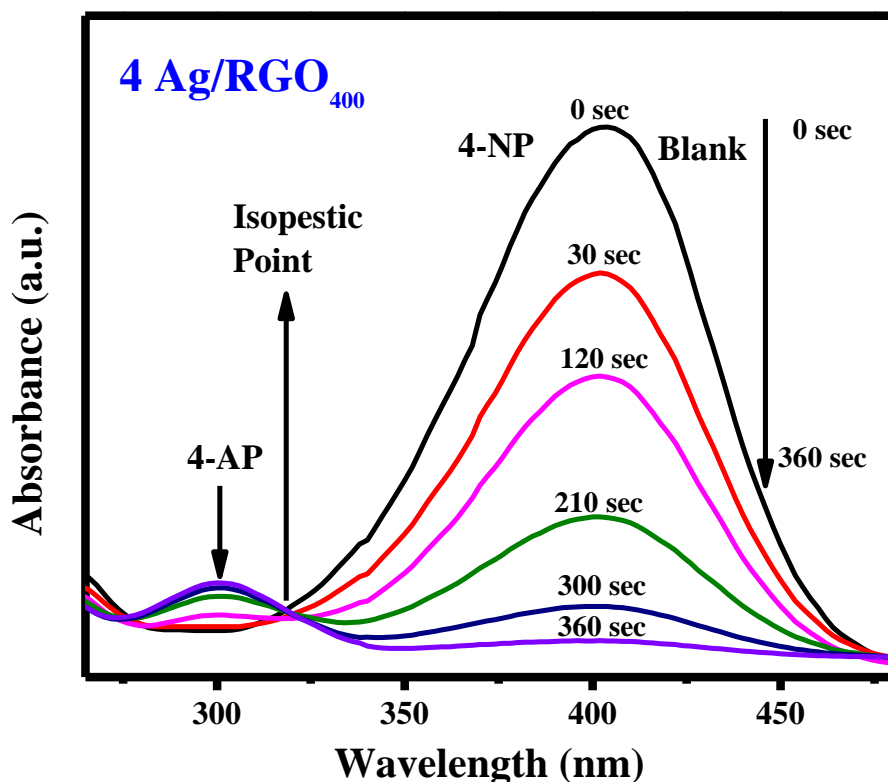


Fig (8): UV–vis absorption spectra of 4-NP before and after adding NaBH₄ and its reduction product 4-AP with time intervals.

Interestingly, this reduction process only takes 360 s for the complete reduction reflecting an excellent catalytic activity of the as-fabricated catalyst. Moreover, a single point of intersection (isopiestic point) was obtained in the UV–vis spectra at 320 nm. This confirms that only one product of 4-AP was produced from the catalytic reduction 4-NP [50, 51].

Fig. 9 shows the relative concentrations of 4-NP remaining in the solutions as a function of time for 0.4Ag/RGO₄₀₀, 4Ag/RGO₂₅₀, and 4Ag/RGO₄₀₀ nanocomposites under dark conditions. In a typical experiment, a 0.025 mg of the catalyst was dispersed in 100 mL of 0.1 mmole 4-NP solution with 12.5 mL of 0.5 mole NaBH₄. It was observed that all the samples show an excellent catalytic activity in the dark toward 4-nitrophenol reduction and the reduction process is accomplished to give

100% conversion in range 360-950 sec for all nanocomposites. This may be due to synergetic effect of the composites components (Ag, Ag₂O and RGO). The efficiency of catalytic reduction of p-nitrophenol has the following order: 4Ag/RGO₄₀₀ > 4Ag/RGO₂₅₀ > 0.4Ag/RGO₄₀₀. The highest reduction activity of the 4% Ag/RGO₄₀₀ catalyst based on the characterization results is attributed to the higher values of pore radius and pore volume in 4Ag/RGO₄₀₀ (18.75 Å, 0.167 cm³/g) compared to rest of catalysts, those facilitate the diffusion of 4-nitrophenol and NaBH₄ molecules on the catalyst surface and thus accelerate their effective interaction. Also, the high crystallinity of sample (confirmed from XRD), low imperfections; as Raman confirms, assists the move of the reactants to the catalyst surface without any obstruction.

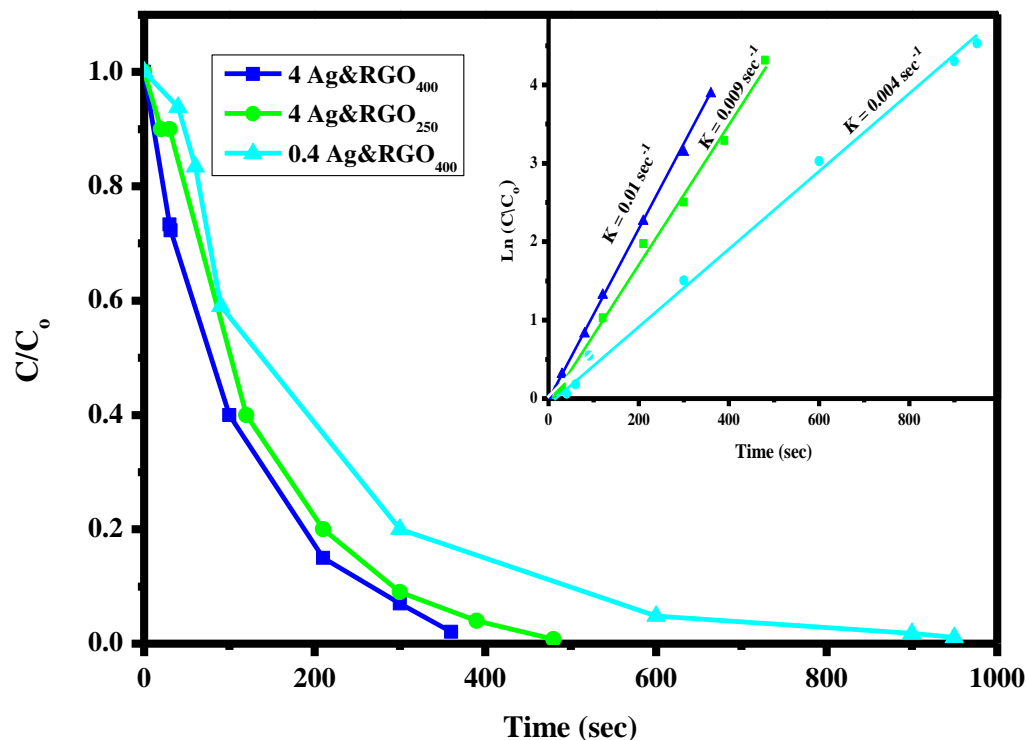


Fig (9): C/C_0 versus time for the hydrogenation of 4-NP over the different catalysts and pseudo-first-order plot of $\ln(C_0/C)$ against reaction time for the hydrogenation of 4-NP over the different catalysts (as inset).

Based on the experimental FTIR, Raman and PL results, the presence of Ag_2O species may have a great effect on the activity. Additionally, 4Ag/RGO₄₀₀ possesses the lowest particle size of 17 nm compared to the other samples as confirmed from TEM results which could be another cause for activating the reaction. Besides, it owns the lowest band gap energy (1.55 eV) explaining the facile electron transfer via this sample.

The inset in Fig. 9 shows the kinetic studies of the catalytic reduction of p-nitrophenol for all Ag/RGO catalysts. It was found that the catalytic reduction follows the Langmuir–Hinshelwood apparent first order kinetics model [52, 53]. The reduction rate constant was computed from the following equation:

$$\ln(C_0/C) = k(t) \quad (2)$$

All the samples show k values in the following order:

4Ag/RGO₄₀₀ (0.01 sec^{-1}) > 4Ag/RGO₂₅₀ (0.009 sec^{-1}) > 0.4Ag/RGO₄₀₀ (0.004 sec^{-1}). The results obtained show that the 4Ag/RGO₄₀₀ sample has the highest rate constant for reduction of p-nitrophenol compared to the other samples. For comparison, the apparent rate constant k_{app} of our sample (4Ag/RGO₄₀₀- in the dark- 0.01 s^{-1}) was much higher than some reported catalysts such as CNFs-AgNPs

($6.02 \times 10^{-3} \text{ s}^{-1}$), Au/partially reduced GO ($8.7 \times 10^{-3} \text{ s}^{-1}$) [54] and AgNP-PG-5K ($5.5 \times 10^{-3} \text{ s}^{-1}$) catalyst [55].

3.7.1. Effect of additives on the catalytic reduction of 4-NP

The presence of some additives either organics or inorganics in water polluted with 4-NP may affect the reduction performance of our catalyst. Thus, reviewing some of these pollutants will give us a clear picture about the catalyst behaviour in their presence and the consequences thereof concerning their influences. Accordingly, the effects of the addition of isopropanol; IPA (a quencher of $\bullet OH$), Na_2CO_3 (H^+ quencher), triethanolamine; TEOA (a quencher of h^+) and benzoquinone; BQ (a quencher of $\bullet O_2^-$), on the catalytic 4-NP reduction over 4%Ag/RGO₄₀₀ of highest activity have been examined under the same experimental conditions. Fig. 10 shows the influence of the mentioned additives in comparison to the absence of any additives on the reaction medium. It was found that the activity decreased for all the additives, however, TEOA and IPA have shown a slight decrease in activity and reached to 100% conversion in a 480 s and 570 s reaction time, respectively, instead of the 100% reduction in 360 s; without additives.

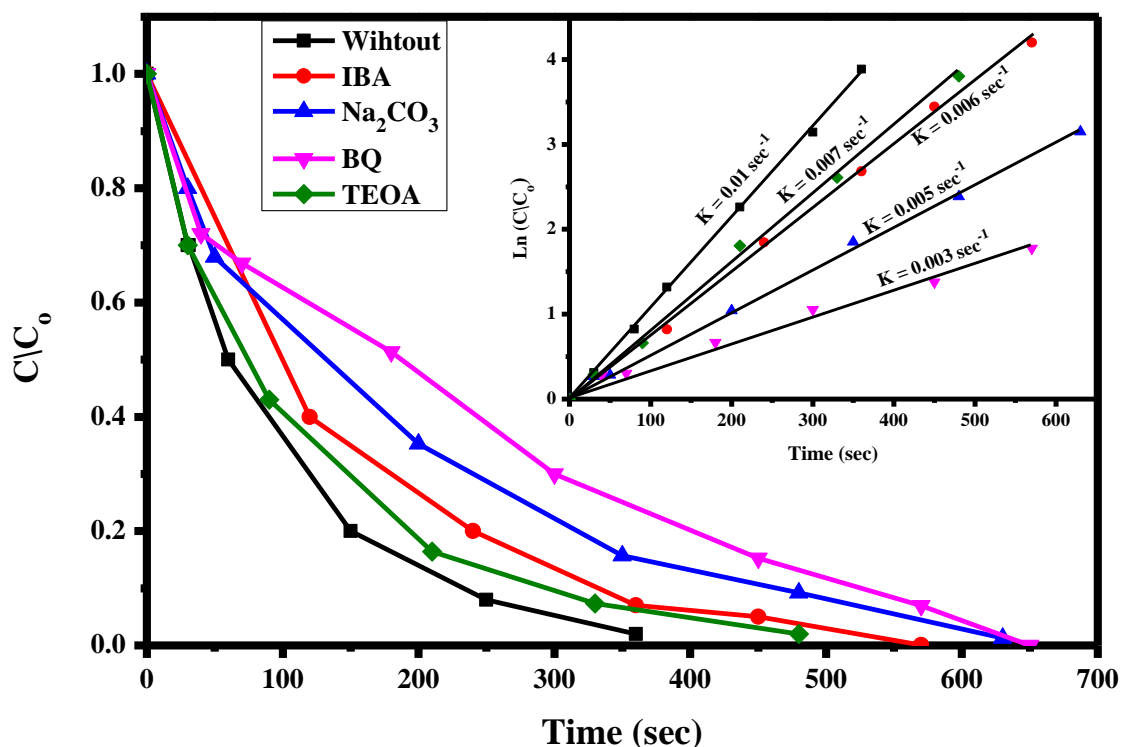


Fig (10): Effect of addition of benzoquinone, isopropyl alcohol, triethanolamine and Na_2CO_3 on the hydrogenation of 4-NP during using 4% $\text{Ag}/\text{RGO}_{400}$ catalyst and $\ln C_0/C$ against time curves as inset.

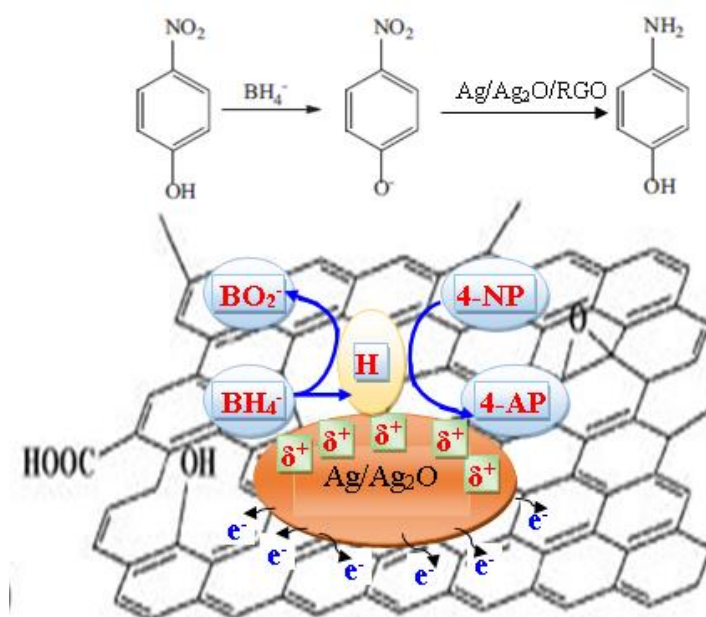
This is because part of NaBH_4 will be depleted for the partial reduction of IPA and TEOA via the hydride ion donation from the nucleophile NaBH_4 to the electrophile O-H of the latter groups. Benzoquinone addition reduces the reduction efficiency of 4-NP to be 100% after 650 s. This kind of delay is a consequence of the hydride ion attack from NaBH_4 to form hydroquinone via the δ^+ carbon atom followed by forming an intermediate with water molecule

3.7.2. Mechanism

After the adsorption of NaBH_4 and 4-nitrophenol on the surface of catalyst particle, the catalytic reduction is started by moving the electrons from the donor BH_4^- (donor) to the acceptor 4-NP molecules. The synergetic effect of Ag, Ag_2O and RGO has great role on the activity of composites. The electron transfer process can be facilitated by Ag nanoparticles on RGO sheet surface of high specific surface area. As shown in scheme 1, due to the strong support-metal interaction (SMSI) effect, some electrons of Ag nanoparticles migrate to the rGO layers, which cause a modifying of the electron density of metal NPs [56]. This transfer process makes the Ag NPs electrophilic. In the presence of BH_4^- , 4-nitrophenolate ions were formed due to deprotonation of 4-NP molecules. The electrophilic Ag NPs prefer to adsorb both the negatively charged 4-

to finally produce alcohols. It was observed that the addition of Na_2CO_3 has the great decrease on the reduction activity to be 100% at ca 700 s. This may be due to the reaction of carbonate with the hydride ion which in consequence decreases the reduction efficiency of NaBH_4 . Conclusively, BQ and Na_2CO_3 delaying the catalytic reduction of 4-NP over $4\text{Ag}/\text{RGO}_{400}$.

Nitrophenolate and BH_4^- ions which facilitate the hydrogenation of 4-nitrophenolate ions on Ag NPs surface [57]. This was in conformity with the kinetic study that follows a Langmuir–Hinshelwood mechanism, in where both reactants are adsorbed on the catalyst prior to reaction progressing [57]. Furthermore, active hydrogen atoms generated through the cleavage of B-H bond over $\text{Ag}/\text{Ag}_2\text{O}$ NPs are formed, via donation of electrons from BH_4^- ions to the electrophilic $\text{Ag}/\text{Ag}_2\text{O}$ NPs [58]. Due to the thermodynamic instability of the active hydrogen atoms they are react readily with 4-nitrophenolate ions. As a result, the promising catalytic activity of $\text{Ag}/\text{Ag}_2\text{O}/\text{rGO}$ can be explained from the facily-created active hydrogen species and the readily reactants adsorbed together with the induced the electron transfer from Ag metals to rGO layers.



scheme (1): Mechanism of catalytic reaction

4. Conclusion

A well dispersion of Ag and Ag₂O nanoparticles on RGO sheets were successfully prepared with different loads and at various annealing temperatures. All nanocomposites exhibit an excellent catalytic conversion of 4-NP to 4-AP. The nanocomposite Ag/RGO with a load of 4% and annealed at 400°C exhibited the highest

reduction rate constant of 4-nitrophenol (4-NP) under the dark (0.01 s⁻¹) and the complete reduction is attained in 360 s only. The catalytic reduction reaction on all composites follows the Langmuir–Hinshelwood apparent first order kinetics model.

References

- [1] K.-C. Hsu and D.-H. Chen, Green synthesis and synergistic catalytic effect of Ag/reduced graphene oxide nanocomposite, *Nanoscale research letters*, 9 (2014) 484.
- [2] H. Hu, J.H. Xin, H. Hu, X. Wang, D. Miao and Y. Liu, Synthesis and stabilization of metal nanocatalysts for reduction reactions—a review, *J. Mater. Chem. A*,3(2015) 11157-11182.
- [3] M. Sharma, A. Mishra, A. Mehta, D. Choudhury and S. Basu, Enhanced catalytic and antibacterial activity of nanocasted mesoporous silver monoliths: kinetic and thermodynamic studies, *J. Sol-Gel Sci. Technol.*,81(2017) 704-710.
- [4] J.-R. Chiou, B.-H. Lai, K.-C. Hsu and D.-H. Chen, One-pot green synthesis of silver/iron oxide composite nanoparticles for 4-nitrophenol reduction, *J. Hazard. Mater.*, 248(2013) 394-400.
- [5] A. Mehta, M. Sharma, A. Kumar and S. Basu, Gold nanoparticles grafted mesoporous silica: a highly efficient and recyclable heterogeneous catalyst for reduction of 4-nitrophenol, *Nano* 16(2016)50104.
- [6] J. Shen, M. Shi, B. Yan, H. Ma, N. Li and M. Ye, One-pot hydrothermal synthesis of Ag-reduced graphene oxide composite with ionic liquid, *J. Mater. Chem.*,21(2011) 7795-7801.
- [7] R. Prucek, J. Tuček, M. Kilianová, A. Panáček, L. Kvítek, J. Filip, M. Kolář, K. Tománková and R. Zbořil, The targeted antibacterial and antifungal properties of magnetic nanocomposite of iron oxide and silver nanoparticles, *Biomaterials* ,32(2011) 4704-4713.
- [8] J.-c. Qu, C.-l. Ren, Y.-l. Dong, Y.-p. Chang, M. Zhou and X.-g. Chen, Facile synthesis of multifunctional graphene oxide/AgNPs-Fe₃O₄ nanocomposite: a highly integrated catalyst, *Biochem. Eng. J.*,211(2012) 412-420.
- [9] H. Sakai, T. Kanda, H. Shibata, T. Ohkubo and M. Abe, Preparation of highly dispersed core/shell-type titania nanocapsules containing a single Ag nanoparticle, *J. Am. Chem. Soc.*,128(2006) 4944-4945.
- [10] L. Chen, D. Ma and X. Bao, Hydrogen treatment-induced surface reconstruction: formation of superoxide species on activated carbon over Ag/activated carbon catalysts for selective oxidation of CO in H₂-rich gases, *J. Phys. Chem. C*,111(2007) 2229-2234.
- [11] N. Tanaka, H. Nishikiori, S. Kubota, M. Endo and T. Fujii, Photochemical deposition of Ag nanoparticles on multiwalled carbon nanotubes, *Carbon*,47(2009) 2752-2754.
- [12] C. Zhu, P. Wang, L. Wang, L. Han and S. Dong, Facile synthesis of two-dimensional graphene/SnO₂/Pt ternary hybrid nanomaterials and their catalytic properties, *Nanoscale*,3(2011) 4376-4382.
- [13] P. Avouris, Z. Chen and V. Perebeinos, Carbon-based electronics, *Nat. nanotechnol.*,2(2007) 605.

- [14] Z. Ji, X. Shen, J. Yang, G. Zhu and K. Chen, A novel reduced graphene oxide/Ag/CeO₂ ternary nanocomposite: Green synthesis and catalytic properties, *Appl. Catal., B: Environ.*,144(2014) 454-461.
- [16] Y. Zhang, X. Yuan, Y. Wang and Y. Chen, One-pot photochemical synthesis of graphene composites uniformly deposited with silver nanoparticles and their high catalytic activity towards the reduction of 2-nitroaniline, *J. Mater. Chem.*,22(2012) 7245-7251.
- [17] T. Wu, S. Liu, Y. Luo, W. Lu, L. Wang and X. Sun, Surface plasmon resonance-induced visible light photocatalytic reduction of graphene oxide: using Ag nanoparticles as a plasmonic photocatalyst, *Nanoscale*,3(2011) 2142-2144.
- [18] E.L. Guerra, A. Shanmugaraj, W. Choi and S.H. Ryu, Thermally reduced graphene oxide-supported nickel catalyst for hydrogen production by propane steam reforming, *Appl. Catal. A: General*,468(2013) 467-474.
- [19] M. Yu, J. Chen, Y. Ma, J. Zhang, J. Liu, S. Li and J. An, Hydrothermal synthesis of NiCo₂O₄ nanowires/nitrogen-doped graphene for high-performance supercapacitor, *Appl. Surf. Sci.*,314(2014) 1000-1006.
- [20] X.-Z. Tang, X. Li, Z. Cao, J. Yang, H. Wang, X. Pu and Z.-Z. Yu, Synthesis of graphene decorated with silver nanoparticles by simultaneous reduction of graphene oxide and silver ions with glucose, *Carbon*,59(2013) 93-99.
- [21] F. Yu, Y. Chen, Y. Wang, C. Liu and W. Ma, Enhanced removal of iodide from aqueous solution by ozonation and subsequent adsorption on Ag-Ag₂O modified on Carbon Spheres *Appl. Surf. Sci.*,427(2018) 753-762.
- [22] X. Zhou, X. Huang, X. Qi, S. Wu, C. Xue, F.Y. Boey, Q. Yan, P. Chen and H. Zhang, In situ synthesis of metal nanoparticles on single-layer graphene oxide and reduced graphene oxide surfaces, *The J. Phys. Chem. C*,113(2009) 10842-10846.
- [23] C. Gómez-Navarro, R.T. Weitz, A.M. Bittner, M. Scolari, A. Mews, M. Burghard and K. Kern, Electronic transport properties of individual chemically reduced graphene oxide sheets, *Nano letters*,7(2007) 3499-3503.
- [24] B. Murray, Q. Li, J. Newberg, E. Menke, J. Hemminger and R. Penner, Shape- and size-selective electrochemical synthesis of dispersed silver (I) oxide colloids, *Nano Lett.*,5(2005) 2319-2324.
- [25] F.H. Chung, Quantitative interpretation of X-ray diffraction patterns of mixtures. I. Matrix-flushing method for quantitative multicomponent analysis, *J. Appl. Crystallogr.*,7(1974) 519-525.
- [26] K.H. Lee, B. Lee, S.-J. Hwang, J.-U. Lee, H. Cheong, O.-S. Kwon, K. Shin and N.H. Hur, Large scale production of highly conductive reduced graphene oxide sheets by a solvent-free low temperature reduction, *Carbon*,69(2014) 327-335.
- [27] C. Cheng, S. Nie, S. Li, H. Peng, H. Yang, L. Ma, S. Sun and C. Zhao, Biopolymer functionalized reduced graphene oxide with enhanced biocompatibility via mussel inspired coatings/anchors, *J. Mater. Chem. B*,1(2013) 265-275.
- [28] V.H. Pham, T.V. Cuong, S.H. Hur, E. Oh, E.J. Kim, E.W. Shin and J.S. Chung, Chemical functionalization of graphene sheets by solvothermal reduction of a graphene oxide suspension in N-methyl-2-pyrrolidone, *J. Mater. Chem.*,21(2011) 3371-3377.
- [29] E. Frackowiak and F. Beguin, Carbon materials for the electrochemical storage of energy in capacitors, *Carbon*,39(2001) 937-950.
- [30] L. Wang, Y. Shi, T. Wang and L. Zhang, Silver chloride enwrapped silver grafted on nitrogen-doped reduced graphene oxide as a highly efficient visible-light-driven photocatalyst, *J. Colloid Interface Sci.*,505(2017) 421-429.
- [31] G.I. Waterhouse, G.A. Bowmaker and J.B. Metson, The thermal decomposition of silver (I, III) oxide: a combined XRD, FT-IR and Raman spectroscopic study, *PCCP*,3(2001)3838-3845.
- [32] M. Khairy and M.M. Mohamed, SnO₂ (β-Bi₂O₃)/Bi₂Sn₂O₇ nanohybrids doped with Pt and Pd nanoparticles: applications in visible light photocatalysis, electrical conductivity and dye-sensitized solar cells, *PCCP*,17(2015) 21716-21728.
- [33] D. Carboni, D. Marongiu, P. Rattu, A. Pinna, H. Amenitsch, M. Casula, A. Marcelli, G. Cibin, P. Falcaro and L. Malfatti, Enhanced photocatalytic activity in low-temperature processed titania mesoporous films, *The J. Phys. Chem. C*,118(2014) 12000-12009.
- [34] F. Zare, M. Ghaedi, A. Daneshfar, S. Agarwal, I. Tyagi, T.A. Saleh and V.K. Gupta, Efficient removal of radioactive uranium from solvent phase using AgOH-MWCNTs nanoparticles: Kinetic and thermodynamic study, *Chem. Eng. J.*,273(2015) 296-306.
- [35] J. Ghilane, F.-R.F. Fan, A.J. Bard and N. Dunwoody, Facile electrochemical characterization of core/shell nanoparticles. Ag core/Ag₂O shell structures, *Nano Lett.*,7(2007) 1406-1412.
- [36] R.V. Hull, L. Li, Y. Xing and C.C. Chusuei, Pt nanoparticle binding on functionalized multiwalled carbon nanotubes, *Chem. Mater.*,18(2006) 1780-1788.
- [37] A.C. Ferrari, J. Meyer, V. Scardaci, C. Casiraghi, M. Lazzeri, F. Mauri, S. Piscanec, D. Jiang, K. Novoselov and S. Roth, Raman spectrum of graphene and graphene layers, *Phys. Rev. Lett.*,97(2006)187401.
- [38] Y. Hao, Y. Wang, L. Wang, Z. Ni, Z. Wang, R. Wang, C.K. Koo, Z. Shen and J.T. Thong, Probing layer number and stacking order of few-layer graphene by Raman spectroscopy, *small*,6(2010) 195-200.
- [39] M. Tajabadi, W. Basirun, F. Lorestani, R. Zakaria, S. Baradaran, Y. Amin, M. Mahmoudian, M. Rezayi and M. Sookhikian, Nitrogen-doped graphene-silver nanodendrites for the non-enzymatic detection of hydrogen peroxide, *Electrochim. Acta*,151(2015) 126-133.
- [40] W. Ouyang, D. Zeng, X. Yu, F. Xie, W. Zhang, J. Chen, J. Yan, F. Xie, L. Wang and H. Meng, Exploring the active sites of nitrogen-doped graphene as catalysts for the oxygen reduction reaction, *Int. J. Hydrogen Energy*,39(2014) 15996-16005.
- [41] Q. Liu, H. Zhang, H. Zhong, S. Zhang and S. Chen, N-doped graphene/carbon composite as non-precious metal electrocatalyst for oxygen reduction reaction, *Electrochim. Acta*,81(2012) 313-320.
- [42] C. Cui, Y. Wang, D. Liang, W. Cui, H. Hu, B. Lu, S. Xu, X. Li, C. Wang and Y. Yang, Photo-assisted synthesis

of Ag₃PO₄/reduced graphene oxide/Ag heterostructure photocatalyst with enhanced photocatalytic activity and stability under visible light, *Appl. Catal. B: Environ.*,158(2014) 150-160.

[43] W.S. Hummers Jr and R.E. Offeman, Preparation of graphitic oxide, *J. Am. Chem. Soc.*,1958,80, 1339-1339.

[44] Q. Huang, J. Wang, W. Wei, Q. Yan, C. Wu and X. Zhu, A facile and green method for synthesis of reduced graphene oxide/Ag hybrids as efficient surface enhanced Raman scattering platforms, *J. Am. Chem. Soc.*,283(2015) 123-130.

[45] H. Hu, Z. Jiao, G. Lu, J. Ye and Y. Bi, Enhanced photocatalytic properties of biomimetic Ag/AgCl heterostructures, *RSC Advances*,4(2014)31795-31798.

[46] M. Jestl, I. Maran, A. Köck, W. Beinstingl and E. Gornik, Polarization-sensitive surface plasmon Schottky detectors, *Opt. Lett.*,14(1989) 719-721.

[47] L. Lin, M. Rong, F. Luo, D. Chen, Y. Wang and X. Chen, Luminescent graphene quantum dots as new fluorescent materials for environmental and biological applications, *TrAC, Trends Anal. Chem.*,83(2014) 83-102.

[48] K. Hayakawa, T. Yoshimura and K. Esumi, Preparation of gold– dendrimer nanocomposites by laser irradiation and their catalytic reduction of 4-nitrophenol, *Langmuir*,19(2003) 5517-5521.

[49] C. Zhijiang, Z. Qin, S. Xianyou, L. Yuanpei and Zein, Poly (3-hydroxybutyrate-co-4-hydroxybutyrate) electrospun blend fiber scaffolds: Preparation, characterization and cytocompatibility, *Mater. Sci. Eng.: C*,71(2017) 797-806.

[50] N. Arora, A. Mehta, A. Mishra and S. Basu, 4-Nitrophenol reduction catalysed by Au-Ag bimetallic nanoparticles supported on LDH: Homogeneous vs. heterogeneous catalysis, *Appl. Clay Sci.*,151(2018) 1-9.

[51] N. Velghe and A. Claeys, Rapid spectrophotometric determination of nitrate with phenol, *Analyst*,108(1983) 1018-1022.

[52] K. Karakas, A. Celebioglu, M. Celebi, T. Uyar and M. Zahmakiran, Nickel nanoparticles decorated on electrospun polycaprolactone/chitosan nanofibers as flexible, highly active and reusable nanocatalyst in the reduction of nitrophenols under mild conditions, *Appl. Catal. B: Environ.*,203(2017) 549-562.

[53] R.W. Scott, C. Sivadinarayana, O.M. Wilson, Z. Yan, D.W. Goodman and R.M. Crooks, Titania-supported PdAu bimetallic catalysts prepared from dendrimer-encapsulated nanoparticle precursors, *J. Am. Chem. Soc.*,127(2005) 1380-1381.

[54] X. Yin, X. Xie, L. Song, J. Zhai, P. Du and J. Xiong, Enhanced performance of flexible dye-sensitized solar cells using flexible Ag@ ZrO₂/C nanofiber film as low-cost counter electrode, *Appl. Surf. Sci.*,24(2018)1243-1250.

[55] B. Baruah, G.J. Gabriel, M.J. Akbashev and M.E. Booher, Facile synthesis of silver nanoparticles stabilized by cationic polynorbornenes and their catalytic activity in 4-nitrophenol reduction, *Langmuir*,29(2013)4225-4234.

[56] L. Liu, R. Chen, W. Liu, J. Wu and D. Gao, Catalytic reduction of 4-nitrophenol over Ni-Pd nanodimers supported on nitrogen-doped reduced graphene oxide, *J. Hazard. Mater.*, 320(2016) 96-104.

[57] Z.D. Pozun, S.E. Rodenbusch, E. Keller, K. Tran, W. Tang, K.J. Stevenson and G. Henkelman, A systematic investigation of p-nitrophenol reduction by bimetallic dendrimer encapsulated nanoparticles, *The J. Phys. Chem. C*,117(2013) 7598-7604.

[58] S. Fountoulaki, V. Daikopoulou, P.L. Gkizis, I. Tamiolakis, G.S. Armatas and I.N. Lykakis, Mechanistic studies of the reduction of nitroarenes by NaBH₄ or hydrosilanes catalyzed by supported gold nanoparticles, *ACS Catalysis*,4(2014) 3504-3511.